Energy transfer in collisions of I^+ with Xe

Pingyi Feng and K. Balasubramanian
Department of Chemistry, Arizona State University, Tempe, Arizona 85287-1604

Joyce J. Kaufman and Walter S. Koski
Department of Chemistry, The Johns Hopkins University, Baltimore, Maryland 21218
(Received 3 November 1989)

Electronic transitions between the spin-orbit states of ^3P and ^1D of I^+ were observed in the inelastic collisions between I^+ and Xe. The Landau-Zener model is used to interpret the transfers of translational energies to electronic energies and vice versa at the crossing points of the various potential-energy curves of $(XeI)^+$. Relativistic complete-active-space self-consistent-field followed by first-order configuration-interaction and relativistic configuration-interaction (RCI) calculations including spin-orbit coupling are carried out on the low-lying electronic states dissociating into $Xe+I^+$ and $Xe^+ + I$ asymptotes. Some of the potential-energy curves correlating into $Xe+I^+$ were found to be bound, while most of the states correlating into $Xe^+ + I$ were found to be repulsive. RCI calculations explain the observed efficient energy transfers. The spin-orbit-corrected RCI D_e of XeI^+ in the 0^+(III) state is calculated as 0.8 eV. Two electronic states of 0^+(II) and 0^+(III) symmetries are found to be strongly bound while 2, 1, and 0^-(I) states are relatively less bound.

I. INTRODUCTION

Energy transfers in rare gas plus halogen ($R+X$) and rare gas plus positively charged halogen (RX^+) collisions and properties of noble-gas halides have been the topics of many recent experimental and theoretical investigations.[1-18] In addition, rare-gas oxides that are isoelectronic with RX^+ have been studied as possible candidates for chemical lasers.[12] Our knowledge of RX^+ species is nevertheless very limited in comparison to information accumulated on RX and rare-gas oxide species.

In hot-atom studies of halogen systems, rare gases have been used as moderators. In these studies the rare-gas atoms are generally assumed to be inert. To the contrary, in recent years collisional studies of X^+ with R for Kr and Br^+ (Ref. 4) as well as Ar and Cl (Ref. 2) have shown that rare-gas atoms actively participate in energy transfer in hot-atom processes. Transfers of translational to electronic energies and vice versa have been observed.

In previous studies we have shown that $KrBr^+$ (Ref. 4) and ArCl (Ref. 2) are well bound and long lived and energy transfers take place between translational and electronic energies in the collisions of Br^+ with Kr and Cl^+ with Ar. It has also been demonstrated through mass-spectrometric methods that XeF^+ and KrF^+ are very stable ions.[17,18] Berkowitz and co-workers[17,18] have examined the binding energies of many RX^+ species such as KrF^+, XeF^+, and XeI^+. In addition to these species the NeF^+ ion was studied by Hotokka *et al.*[1] using both experimental techniques and theoretical complete-active-space self-consistent-field (CASSCF) calculations.

In the present investigation, we carry out both experimental and theoretical studies on energy transfers in the $Xe+I^+$ collisions. Collisions of such heavy species are very interesting from a theoretical standpoint due to large relativistic effects. In addition, spin-orbit effects become quite significant, especially for $Xe+I^+$ collisions. Thus the present study is aimed at shedding light on basic relativistic effects on the nature of electric states and the nature of energy transfers in $Xe+I^+$ collisions.

Section II describes the experimental results and the experimental method of the studies. Section III outlines the theoretical method of calculations. Section IV comprises results and discussions on potential-energy curves, binding energies, and energy transfers. Section V discusses the nature of the various electronic states studied, including the effect of spin-orbit coupling and avoided crossings, etc.

II. EXPERIMENTAL METHODS AND RESULTS

An energy-level diagram at infinite separation for the Xe-I^+ system is shown in Fig. 1. The maximum kinetic energy involved in the present studies is only 5 eV and thus only the $^1D_2$ and $^3P_{2,1,0}$ spin-orbit states of I^+ are accessible. The energy transfers studied here can thus be represented by the following equations:

$$I^+(^3P)+Xe(^1S)\leftrightarrows I^+(^1D)+Xe(^2S)\ .$$

Among the possible electronic transfers only the $I^+(^3P_{0,1})\leftrightarrows I^+(^1D_2)$ transitions are observed. The $I^+(^3P_2)\leftrightarrows I^+(^1D_2)$ transition is apparently not observed.

If the energy-transfer processes in these collisions are governed by a Landau-Zener model, then the potential-energy curves of the intermediate XeI^+ complex will be useful to understand the channels for the formation of XeI^+ and to comprehend why $I^+(^3P_1,^3P_0)\leftrightarrows I^+(^1D_2)$ transitions are observed while the $I^+(^3P_2)\rightleftarrows I^+(^1D_2)$ collisional transition cannot be observed.

Collisions of I^+ with Xe were measured using a tandem mass spectrometer, which has been described previ-

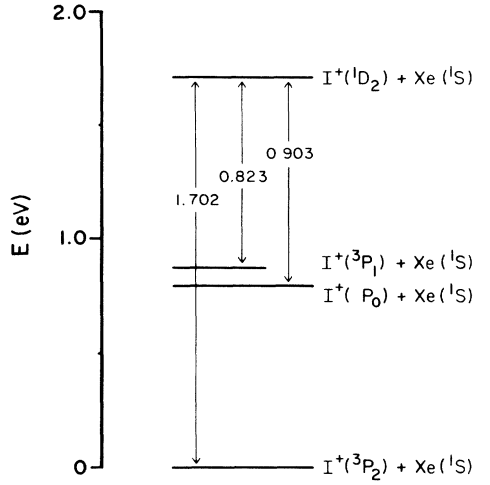

FIG. 1. Energy-level diagrams for $I^+ + Xe$ at infinite separation. Experimentally only $I^+(^3P_{0,1}) \leftrightarrow I^+(^1D_2)$ transitions are observed. The $I^+(^3P_2) \leftrightarrows I^+(^1D_2)$ transition could not be observed.

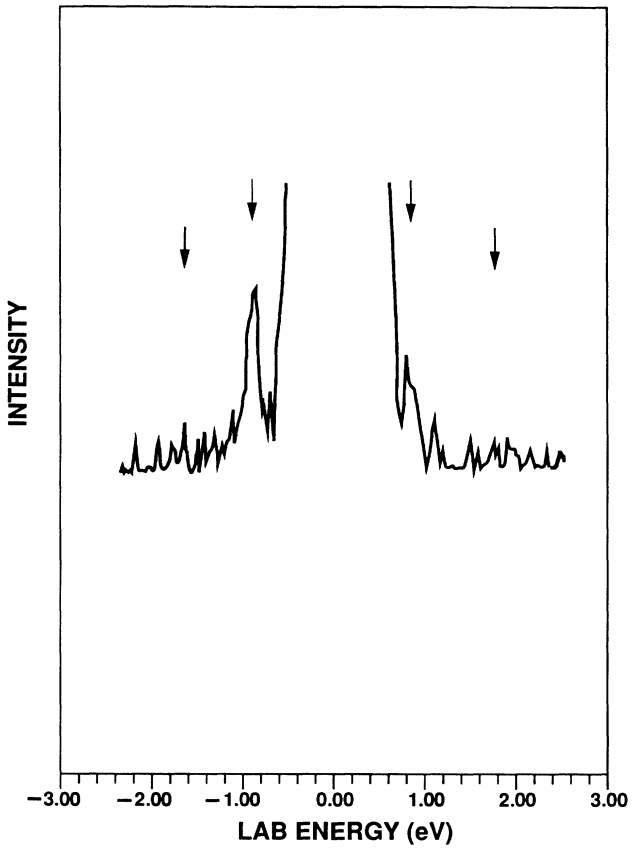

FIG. 2. Kinetic-energy spectra of I^+ resulting from $I^+ + Xe$ collisions at 5-eV center-of-mass energy. Arrows indicate where peaks may be expected.

ously.[6] It consists of an ion source, an electrostatic analyzer, and a quadrupole mass spectrometer as an input section The ions were prepared by 100-eV electron bombardment of CH_3I. The beam composition so produced has 25% $I^+(^1D_2)$ and 75% $I^+(^3P_{2,1,0})$ as determined by attenuation measurements of I^+ in xenon. The beam width was 0.1 eV in energy and 1.5° in angle [both full width at half maximum (FWHM)].

The I^+ ion beam from this section was passed through a shallow reaction chamber containing the target gas Xe. The experiments were carried out under thin target conditions. The I^+ ions scattered at 0° to the beam direction were then detected with a second quadrupole mass spectrometer followed by an electrostatic analyzer and an electron multiplier.

In this way, an energy spectrum of the forward-scattered I^+ was obtained (Fig. 2). The cross section for the energy-transfer process in the I^+-Xe system was qualitatively much smaller than that in the F^+-Ne system[1] and consequently, the signal-to-noise ratio is much poorer. The intense central peak is the unperturbed I^+. The satellite peaks on each side of the primary are separated from the main peak by approximately 0.86 eV. The "superelastic" peak on the right corresponds to the transition $I^+(^1D_2) \rightarrow I^+(^3P_{0,1})$ and the more intense "subelastic" satellite on the left is due to the transition $I^+(^3P_{0,1}) \rightarrow I^+(^1D_2)$. The levels corresponding to $^3P_1$ and $^3P_0$ are separated by only 80 meV and apparently are not resolved in the measurement. The transitions $^3P_2 \rightleftarrows {}^1D_2$ are apparently not observed and their expected positions are indicated by arrows in Fig. 2. A similar situation was observed in the $BrKr^+$ system Admittedly, because of the unfavorable signal-to-noise ratio, if the signal corresponding to this transition was only a quarter of the amplitude of the $I^+(^3P_{0,1}) \rightleftarrows I^+(^1D_2)$ transition we probably would not detect it. However, if one examines the potential-energy diagram, it is clear that the curves correlating with $^1S_0 + {}^3P_2$ are well removed from the curves associated with $^1S_0 + {}^1D_2$, so it is very likely that the transitions $^3P_2 \rightleftarrows {}^1D_2$ do not occur. Similarly, the possible transitions $^3P_2 \rightleftarrows {}^3P_{0,1}$ would be difficult to distinguish experimentally from the transitions $^3P_{0,1} \rightleftarrows {}^1D_2$ since their energies are closed and again, an examination of the potential energy shows that the curves correlating with $^1S_0 + {}^3P_{1,0}$ are well separated from those correlating with $^1S_0 + {}^3P_2$, so these transitions in all likelihood are not taking place. It is probably worthy of comment that the observed low signal-to-noise ratio arises in part from the expected low transition probability at crossing of the 1(II) and 0^+(III) curves.

Various rare-gas–halogen ions ($ArCl^+$,[2] $KrBr^+$,[4] etc.) are readily prepared by the electron bombardment of a mixture of the rare gas and a suitable halogen containing molecules at pressures of 1 Torr or higher. Following the same procedure we irradiated a 50:50 Xe-CH_3I mixture with 100-eV electrons. The XeI^+ ion was readily observed indicating that it had a lifetime greater than 700 μsec, the transit time in our instrument.

In summary of the experimental measurements it was found that under binary collisions conditions inelastic collisions of I^+ and Xe results in energy transfers corresponding to the transitions $I^+(^3P_{0,1}) \leftrightarrows I^+(^1D_2)$, but apparently no energy transfers corresponding to $I^+(^3P_2) \leftrightarrows I^+(^1D_2)$ were observed.

TABLE I. A few low-lying configurations of XeI^+ and the corresponding λ-s and ω-ω states arising from them.

Electronic configurations	λ-s states	ω-ω states
$\sigma^2\sigma^*\pi^4\pi^{*3}$	$^3\Pi$	$2,1,0^-,0^+$
	$^1\Pi$	1
$\sigma^2\pi^4\pi^{*4}$	$^1\Sigma^+$	0^+
$\sigma^2\sigma^{*2}\pi^4\pi^{*2}$	$^3\Sigma^-$	$0^+,1$
	$^1\Delta$	2
	$^1\Sigma^+$	0^+
$\sigma^2\sigma^{*2}\pi^3\pi^{*3}$	$^3\Sigma^-$	$0^+,1$
	$^3\Sigma^+$	$0^-,1$
	$^3\Delta$	3,2,1
	$^1\Sigma^+$	0^+
	$^1\Sigma^-$	0^-
	$^1\Delta$	2

III. THEORETICAL METHOD OF CALCULATIONS FOR $(XeI)^+$

We assume that the energy transfers can be modeled by a Landau-Zener type of process and in order to interpret the experimental results it is necessary to have some knowledge of the Xe-I^+ potential-energy curves. In this section we present the results of quantum-chemical calculations of these curves.

We carried out CASSCF multiconfiguration self-consistent-field (MCSCF) calculations followed by first-order configuration-interaction (FOCI) calculations. These calculations were subsequently followed by relativistic CI (RCI) calculations, which included both electron correlation effects and spin-orbit effects simultaneously.

Relativistic effective core potentials which included the outer $5s^25p^6$ shells of Xe and $5s^25p^5$ shell of the I atom were employed. A valence Gaussian basis set of $(4s4p2s)$ quality was employed. We started with the $(3s3p)$ valence Gaussian basis sets optimized by La John *et al.*[19] for Xe and I. To this, one set of s and p diffuse functions and two sets of six-component $3d$-type functions were added. Thus the resulting basis set is large enough and has adequate flexibility.

At the CASSCF level, all valence electrons of XeI^+ (14 outer electrons) were distributed in all possible ways among those orbitals which correlated into Xe($5s$), Xe($5p$), I($5s$), and I($5p$) at infinite separation. All calculations were carried out in the C_{2v} symmetry group orienting the molecule along the z axis. In this orientation, the active space of orbitals for the CASSCF spanned four a_1, two b_2, and two b_1 orbitals. These orbitals correlate into Xe($5s$), Xe($5p$), I($5s$), and I($5p$) at infinite separation.

Following CASSCF calculations CI calculations were carried out using the FOCI methodology. The FOCI calculations included all configurations in the CASSCF plus those configurations obtained by distributing 13 electrons in the internal space, one electron in the external space in all possible ways. The CASSCF calculations included up to 16 configurations, while the FOCI calculations included up to 2700 configurations. The CASSCF-FOCI procedure thus takes into account electron correlation effects.

Spin-orbit effects are definitely expected to be large for XeI^+ since I^+ has a large spin-orbit coupling. The spin-orbit coupling was introduced variationally through a RCI scheme. In this method all low-lying states of the same Ω symmetry are mixed in the presence of spin-orbit integrals. Table I show possible low-lying states of $(XeI)^+$ in both λ-s and ω-ω couplings. As seen from that table, there are many states for $(XeI)^+$. In an earlier study on $KrBr^+$,[4] we outlined in detail the selection of reference configurations for various states in the ω-ω coupling. We used the same procedure for the choice of reference configurations in the RCI. Subsequently, single and double excitations were allowed for all the reference configurations in the RCI. Hence RCI is a multireference single plus double CI (MRSDCI) method including the spin-orbit coupling. All CASSCF-FOCI calculations were made using a modified version[20] of ALCHEMY II codes[21] as described in Ref. 20. Spin-orbit integrals were calculated using Pitzer's modified version of ARGOS.[22] RCI calculations were done using Balasubramanian's RCI codes for polyatomic molecules described in Ref. 23.

IV. RESULTS AND DISCUSSION

Table II shows theoretical asymptotic energy separations of $Xe+I^+$ at long distances as obtained from our calculations and the corresponding experimental values. As seen from Table II the agreement between theoretical separations of spin-orbit states of I^+ and the corresponding experimental values is remarkable for $^3P_2$-$^3P_1$, $^3P_2$-$^3P_0$ separations. We consider this fortuitous since the level of theory is not of the accuracy implied by Table II. The $^3P_2$-$^1D_2$ theoretical energy separation is higher than the experimental value. This trend is consistent with earlier calculations on $Kr+Br^+$ collisions for which the Br^+ $^3P_2$-$^1D_2$ energy separation was calculated as 14 639 cm^{-1} compared to an experimental value of 11 409 cm^{-1}.[24] The most probable cause for this

TABLE II. Dissociation limits of a few low-lying ω-ω states of $(XeI)^+$.

Molecular states	Dissociation limit $Xe+I^+$	Energy of the separate atoms (cm^{-1}) Theory	Expt.
$2,1,0^+(I)$	$^1S_0+^3P_2$	0.0	0.0
$1(II),0^-$	$^1S_0+^3P_1$	6913	7090
$0^+(II)$	$^1S_0+^3P_0$	6428	6451
$2(II),1(III),0^+(III)$	$^1S_0+^1D_2$	16 000	13 731

discrepancy is an incomplete treatment of electron correlation, which tends to predict a lower ^3P energy relative to ^1D.

The usual ordering of an inverted ^3P state is $^3P_2$, $^2P_1$, and $^3P_0$. This order is adhered to by the Br^+ Cl^+ ions while for I^+, $^3P_0$ is lower than $^3P_1$ as seen from Table II. The main reason for the lowering of $^3P_0$ relative to $^3P_1$ is due to spin-orbit mixing of the $^3P_0$ state of I^+ with $^1S_0$ state arising from the same $5p^4$ configuration. It is interesting to note that for the isoelectronic Te atom also $^3P_2$-$^3P_1$ and $^3P_2$-$^3P_0$ separations are 4751 and 4707 cm^{-1}.[22] The $^3P_2$ state is contaminated with $^1D_2$, while $^3P_0$ mixes with $^1S_0$. However, the $^3P_1$ state is relatively pure as there is no low-lying $J=1$ state to cause contamination with $^3P_1$.

Table II also shows possible low-lying ω-ω states of XeI^+ arising from $Xe+I^+$ collisions. We decided to investigate all states correlating into $Xe(^1S_0)+I^+(^3P_{2,1,0};^1D_2)$ limits. Potential-energy curves arising from $Xe^+ + I$ states are also obtained in the absence of spin-orbit coupling, but all the states studied here correlating into this limit were found to be repulsive.

Figure 3 shows potential-energy curves arising from the collisions of $Xe(^1S_g)+I^+(^3P_g)$, $Xe(^1S_g)+I^+(1^{D_g})$, and $Xe^+(^2P_u)+I(^2P_u)$ in the absence of spin-orbit interactions. While these curves are not accurate or real in the sense that they do not include spin-orbit effects, these curves are very useful in our understanding of avoided crossings and other features in the potential-energy curves, which includes spin-orbit effects.

All curves obtained here dissociating into $I+Xe^+$ charge-transfer states of $(XeI)^+$ are repulsive. This is not surprising and is fully consistent with our earlier comparable calculations on the $(ArCl)^+$ ion[2] for which $^1\Sigma^+$(II), $^3\Pi$(II), and $^1\Pi$(II) curves were found to be repulsive. Hence these states were not considered further.

RCI calculations were carried out on potential-energy curves of $(XeI)^+$ including spin-orbit effects for states correlating into $Xe(^1S_0)+I^+(^3P_{2,1,0};^1D_2)$ limits. In all nine ω-ω electronic states were considered including spin-orbit effects.

As seen from Fig. 3, the $^3\Pi$ curve dissociating into $I^+(^3P_g)+Xe(^1S_g)$ has a shallow long-range minimum while the $^3\Sigma^-$ curve dissociating into the same limit is repulsive. Two of the three states dissociating into the $I^+(^1D)+Xe(^1S)$ limit are bound. The $^1\Sigma^+$ state correlating into $I^+(^1D)+Xe(^1S)$ is especially strongly bound with a D_e of 1.78 eV in the absence of spin-orbit coupling. In fact, the $^1\Sigma^+$ state is only 760 cm^{-1} above the $^3\Pi$ state in the absence of spin-orbit coupling for XeI^+. However, as we discuss below, spin-orbit effects destabilize the bond. This is reminiscent of isoelectronic I_2 for which Li and Balasubramanian[25] showed that spin-orbit coupling decreases D_e substantially.

Figure 4 shows potential-energy curves of nine electronic states of $(XeI)^+$, which include the effects of spin-orbit coupling. As seen from Fig. 4, potential-energy curves obtained including spin-orbit effects differ substantially from the corresponding curves without spin-orbit coupling shown in Fig. 3. These differences were mainly due to $^3\Pi$-$^1\Sigma^+$, $^3\Sigma^-$-$^1\Sigma^+$, $^3\Sigma^-$-$^1\Pi$ curve crossings in Fig. 3, which resulted in avoided crossings of the corresponding Ω states of the same symmetry such as 0^+ and 1 states.

As seen from Fig. 4, the 2 and 1 curves are weakly

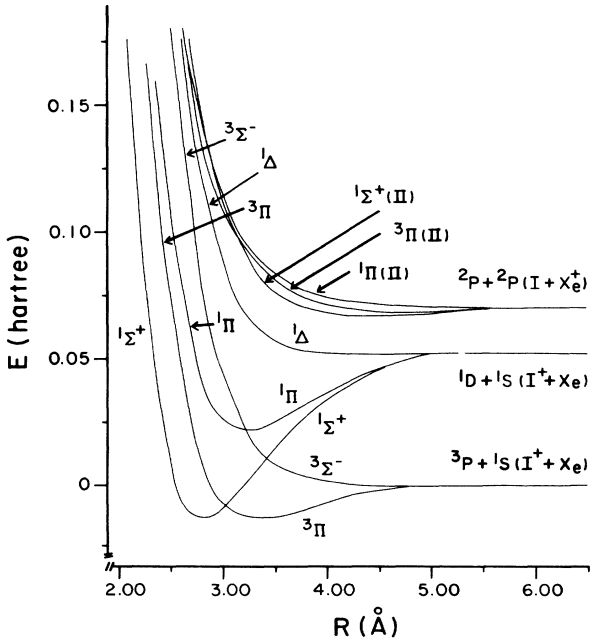

FIG. 3. Potential-energy curves of $(XeI)^+$ arising from $Xe+I^+$ and $Xe^+ + I$ collisions without spin-orbit effects.

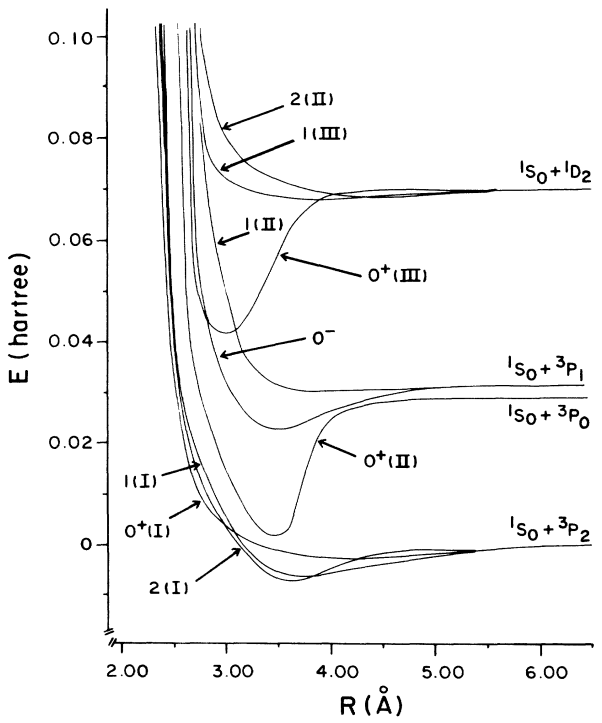

FIG. 4. Potential-energy curves of XeI^+ including spin-orbit effects arising from $Xe(^1S_0)+I^+(^3P_2)$, $Xe(^1S_0)+I^+(^3P_1)$, $Xe(^1S_0)+I^+(^3P_0)$, and $Xe(^1S_0)+I^+(^1D_2)$ collisions.

bound while the O^+(I) curve is mostly repulsive. All of these curves go into the same $Xe(^1S_0)+I^+(^3P_2)$ limit as anticipated from Wigner-Witmer rules.

The 0^+(II) curve dissociating into $Xe(^1S_0)+I^+(^3P_0)$ is bound with respect to this limit. This curve for $(XeI)^+$ is more bound compared to $(KrBr)^+$ partly because the $I^+(^3P_2)$-$I^+(^3P_0)$ separation is higher than the $Br^+(^3P_2)$-$Br^+(^3P_0)$ separation. The 0^- state dissociating into $Xe(^1S_0)+I^+(^3P_1)$ is also bound but somewhat less compared to the 0^+(II) state. The 1(II) state is predominantly repulsive.

The 0^+(III) curve is the most bound of all the low-lying electronic states of XeI^+. The nature of this state changes as a function of internuclear distances due to many avoided crossings. This state dissociates into $Xe(^1S_0)+I^+(^1D_2)$. The other two curves dissociating into $Xe(^1S_0)+I^+(^1D_2)$[2(II),1(III)] are primarily repulsive.

As noted before experimentally, $I^+(^1D_2)\leftrightarrows I^+(^3P_0)$ and $I^+(^1D_2)\leftrightarrows I^+(^3P_1)$ transitions have been observed in the collisions of Xe and I^+. If one models the translational to electron energy transfers by the Landau-Zener model, then efficient energy transfer takes place at the points of intersection of appropriate potential-energy curves. As seen from Fig. 4, during the collision of $Xe(^1S_0)+I^+(^1D_2)$, the 0^+(III) bound state of XeI^+ can be formed. This state is crossed by the 0^- and 1(II) curves. If the predissociation selection rule is applicable for the energy-transfer process, the 0^+(III) state will survive crossing of the repulsive 0^- state since a $+\leftrightarrow-$ transition is forbidden. However, the crossing of the 1(II) repulsive curve with 0^+(III) will provide a channel for energy transfer of the 0^+(III) state formed by collision of $Xe(^1S_0)+I^+(^1D_2)$ to dissociate into $Xe(^1S_0)+I^+(^3P_1)$. Thus the most efficient energy-transfer channel for $I^+(^1D_2)\leftrightarrows I^+(^3P_1)$ should be through the 1(II) channel. The $^3P_0$-$^3P_1$ separation is rather small and clearly the 0^+(II) and 1(II) curves come very close to each other at 4.25 Å. Hence, although they do not exactly cross, the near proximity of these two curves should provide for the interaction of the 0^+(II) and 1(II) states, thereby providing an indirect channel for the conversion of 0^+(III) through the interaction with 1(II). This facilitates the $I^+(^1D_2)\rightleftarrows I^+(^3P_0)$ transition. Note that the 0^+(III) and 0^+(II) states avoid each other as these states are of the same Ω symmetry.

All three curves dissociating into $Xe(^1S_0)+I^+(^3P_2)$ are energetically apart from those states dissociating into $Xe(^1S_0)+I^+(^1D_2)$ or $Xe(^1S_0)+I^+(^3P_1)$. Only the 0^+(II) curve near its r_e comes closer to 0^+(I), but these states avoid each other. Since 0^+(II) stays above the three repulsive curves dissociating into $Xe(^1S_0)+I^+(^3P_2)$, there is no possibility of the vibrational levels of the 0^+(II) state interacting with the vibrational levels of weakly bound 2 and 1 states. This explains why the $I^+(^1D_2)\rightleftarrows I^+(^3P_2)$ transition could not be observed experimentally. It has been suggested to us that because of the comparatively high velocity at the crossing point of the 1(II) and 0^+(III) curves, the Landau-Zener (LZ) transition probability is vanishingly small and hence some other explanation for the energy transfer is called for. A rough estimate of the transition probability can be obtained from the LZ equation $P=2\pi V_{12}/\hbar v_R \Delta F$. At 5-eV center-of-mass energy the velocity in atomic units is $v_0=1.25\times10^{-3}$. We convert this to radial velocity at the crossing point using the expression $v_R\approx v_0(1-b^2/R_\chi^2)^{1/2}$ and for typical b's (impact parameter) around $\frac{3}{4}$ of R_χ we get $v_R\approx v_0/2$. ΔF, the difference of the slopes of the 1(II) and 0^+(III) curves at the crossing point, can be obtained from the calculated potential-energy curves as 0.163 au. R_χ is the internuclear distance at the crossing point. The transfer apparently proceeds through rotational coupling. The operator is $\dot\theta L_y$, where y is the rotation axis. $\dot\theta_{R_\chi}=(v_0/R_\chi)(b/R_\chi)$ and again we take $b/R_\chi\sim\frac{3}{4}$. The order of magnitude of the Ly matrix element is $\hbar$. Substituting these in the LZ equation and recalling that transitions also occur on the way out, we obtain, on average, a transition probability of 3.2×10^{-3}. This probability is small but not negligible and probably accounts for the low signal-to-noise ratio observed. This low transition probability can be detected because in these energy-transfer reactions involving halogen positive ions and rare-gas atoms the distribution of the observed ions is not isotropic but rather the differential cross section is sharply peaked in the forward direction, producing a focusing effect which increases the number of detected ions significantly. We have discussed this point at some length in a previous publication.[1]

The lifetimes of various bound states depend on the classical regions of predissociation due to repulsive curve crossings. If the point of crossing of a repulsive state occurs above the classical turning points of a vibrational level, then the species can have long lifetimes in that vibrational level. Hence the number of vibrational levels with classical turning points below the curve crossing determine the lifetimes of various states. For example, the 0^+(III) state is crossed by the 1(II) curve at a distance longer than R_e of the 0^+(III) curve. We expect only two to three vibrational levels below the 0^+(III)-1(II) curve crossing. Thus the 0^+(III) state may not be very long lived depending on the relative kinetic energy of colliding species.

The 0^+(II) curve is bound and is not crossed by any repulsive curve. Thus the 0^+(II) state will have very long lifetimes. This explains why $(XeI)^+$ is experimentally observed to be a long-lived species.

The direct RCI D_e of the 0^+(III) state with respect to $Xe(^1S_0+I^+(^1D_2)$ is 0.78 eV. The corresponding binding energy of the $^1\Sigma^+$ state dissociating into $Xe(^1S_g)+I^+(^1D_g)$ is 1.78 eV. Thus D_e is significantly altered, although we believe that RCI calculations do not include

TABLE III. Spectroscopic properties of low-lying states of XeI^+.

State	R_e (Å)	T_e (cm^{-1})	ω_e (cm^{-1})	D_e (eV)
$^3\Pi$	3.30	0	155	0.36
$^1\Sigma^+$	2.84	720	202	1.77
$^1\Pi$	3.26	7831	158	0.84

TABLE IV. Electronic properties of some RCI states of XeI^+.

State	R_e (Å)	T_e (cm^{-1})	D_e (eV)
2(I)	3.62	0	0.24
1(I)	3.73	90	0.18
0^+(I)	3.48	1567	0.78
0^-	3.35	6393	0.25
0^+(III)	3.01	10 155	0.78

electron correlation effects to a high order and hence the experimental D_e of the 0^+(III) state should be larger than 0.78 eV. Allowing for the correction to D_e from higher-order electron correlation effects, a value of 1 ± 0.2 eV is predicted as the $D_e(XeI)^+$.

The large D_e of 1.78 eV obtained for the $^1\Sigma^+$ state without spin-orbit coupling is divided between the 0^+(III) and 0^+(II) states as seen from Fig. 4. As we discuss in Sec. V there are many avoided crossings in the 0^+ curves. Hence the $^3\Pi$ curve, which is weakly bound, yields a more strongly bound 0^+(II) state, while the $^1\Sigma^+$ state, which is strongly bound, yields a less stable 0^+(III) curve. Hence the D_e of the 0^+(II) state is enhanced also to about 0.78 eV. Thus the 0^+(II) and 0^+(III) states are nearly equally bound, but we believe that RCI calculations underestimate the binding energy of 0^+(III) and overestimate the D_e of 0^+(II). We predict the D_e of the 0^+(III) and 0^+(II) states to be $1.0\pm.2$ and 0.7 ± 0.2 eV, respectively.

Table III shows spectroscopic constants for XeI^+ in the absence of spin-orbit coupling, while Table IV shows the corresponding constants from RCI calculations including spin-orbit effects. As seen from Table III, in the absence of spin-orbit coupling the $^3\Pi$ state is the ground state of XeI^+ with $R_e=3.30$ Å. The ω_e of the low-lying bound states are between 155 and 200 cm^{-1}. It is interesting to note that the $^1\Sigma^+$ state of XeI^+ exhibits a remarkable resemblance to the $^1\Sigma_g^+$ ground state of isoelectronic I_2. For I_2 earlier theoretical calculations by Li and Balasubramanian[25] indicated excellent agreement of theoretical results with experimental $R_e=2.666$ Å and $\omega_e=214.5$ cm^{-1}. Note that R_e and ω_e of the $^1\Sigma^+$ state are 2.84 Å and 202 cm^{-1}. The bond length is expected to be longer than its true value at the FOCI level. At a higher level a bond length of 2.7–2.75 Å is predicted, making it closer to the properties of the $^1\Sigma_g^+$ state of I_2.

As seen from Table IV, the electronic properties of low-lying states of XeI^+ obtained from RCI calculations, which included spin-orbit coupling, are quite different. This is primarily due to spin-orbit mixing of different λ-s states with the same Ω symmetry. As seen from Table IV, the ground state of $(XeI)^+$ is a 2 state with a long R_e and a D_e of 0.24 eV. The 1 state is, however, nearly degenerate with the 2 state. The R_e of the 0^+(II) is increased mainly due to mixing of the $^1\Sigma^+$ state with the $^3\Pi_{0^+}$ and $^3\Sigma_{0^+}^-$ states. Thus D_e is also reduced considerably for the 0^+(III) state.

V. THE NATURE OF LOW-LYING STATES OF $(XeI)^+$

Table V shows Mulliken population analyses of FOCI natural orbitals for three bound states of $(XeI)^+$ in the absence of spin-orbit coupling. As seen from Table V, the $^3\Pi$ ground state dissociating into $Xe(^1S_g)+I^+(^3P_g)$ behaves very differently from the $^1\Sigma^+$ and $^1\Pi$ states, both of which dissociate into $Xe(^1S_g)+I^+(^1D_g)$. The main difference is in the considerably larger Xe total population in the $^3\Pi$ state. The $^3\Sigma^-$ state, which is repulsive, behaves akin to $^3\Pi$. As evidenced from Table V, there is 0.32 electronic charge transfer from Xe to I in the $^1\Sigma^+$ state compared with $^3\Pi$. Alternatively, 21% of the positive charge resides on Xe while the remaining 79% of the charge resides on I in the $^3\Pi$ state. In the $^1\Sigma^+$ state the positive charge is divided more equitably in that 53.5% of the charge is on Xe while the remaining 46.5% of the charge is on I. In the $^1\Pi$ state 44% of the charge is on Xe while the remaining 56% is on I. Evidently, there is more charge transfer in the $^1\Sigma^+$ and $^1\Pi$ states.

The individual s and p populations on two centers are also of interest. As seen from Table V, the gross s populations of both Xe and I are closer to 2.0, indicating that the $5s^2$ shells of the two atoms are relatively inert. The $5p$ populations on two centers suggest that most of the electronic population lost upon ionization comes from I in the $^3\Pi$ state. The $^3\Sigma^-$ state not shown in Table V exhibited a similar behavior. In the $^1\Sigma^+$ and $^1\Pi$ states the p populations of both Xe and I atoms are nearly equal, indicating an equitable split of charge.

The Xe-I overlap populations measure the approximate bond strengths in the absence of spin-orbit coupling. As seen from Table V, the Xe-I overlaps are somewhat small in the $^3\Pi$ and $^1\Pi$ states, indicating the weakly bound nature of these states in the absence of spin-orbit effects. The $^1\Sigma^+$ state has considerably larger Xe-I overlap population.

The effect of spin-orbit coupling on the shapes of potential-energy curves of $(XeI)^+$ as a function of internuclear distance is quite interesting. Table VI shows weights of leading configurations in the RCI wave functions of low-lying states of $(XeI)^+$ as a function of internuclear distance. Particular attention is drawn to the composition of 0^+, 0^+(II), and 0^+(III) states as a func-

TABLE V. Mulliken population analysis for low-lying states of XeI^+.

		Gross population						
State	R (Å)	Xe	I	Xe(s)	Xe(p)	I(s)	I(p)	Overlap
$^3\Pi$	3.50	7.788	6.212	2.016	5.769	1.994	4.193	0.074
$^1\Sigma^+$	2.84	7.465	6.535	1.961	5.401	1.954	4.511	0.26
$^1\Pi$	3.30	7.559	6.441	2.016	5.525	1.995	4.420	0.083

tion of distance. This table should be used in conjunction with Figs. 3 and 4.

As seen from Table VI, the lowest 0^+ state, namely 0^+(I), is predominantly $^1\Sigma^+$ at 2.50 Å. This is consistent with Fig. 3, which shows that $^1\Sigma^+$ is lower than $^3\Pi$ and $^3\Sigma^-$ at $R=2.5$ Å. Hence the 0^+(I) state is $^1\Sigma^+$ at 2.50 Å, while the 0^+(II) and 0^+(III) states are $^3\Pi_{0^+}$ and $^3\Sigma^-_{0^+}$, respectively. At 2.75 Å, the interaction between $^3\Pi$ and $^1\Sigma^+$ becomes larger. At $R>3.00$ Å, as seen from Fig. 3, the $^1\Sigma^+$ curve crosses with $^3\Pi$. This induces an avoided

TABLE VI. Weights (%) of important electronic configurations in the RCI wave functions of XeI^+.

State	R (Å)	Electronic configuration (% of contribution)
0^+(I)	2.50	$3\sigma^2\pi^4\pi^{*4}$, $^1\Sigma^+_{0^+}$ (92.5)
	2.75	$3\sigma^2\pi^4\pi^{*4}$, $^1\Sigma^+_{0^+}$ (81.5); $3\sigma^24\sigma^*\pi^4\pi^{*3}$, $^3\Pi_{0^+}$ (12)
	3.00	$3\sigma^2\pi^4\pi^{*4}$, $^1\Sigma^+_{0^+}$ (53.6); $3\sigma^24\sigma^*\pi^4\pi^{*3}$, $^3\Pi_{0^+}$ (38.4); $3\sigma^24\sigma^{*2}\pi^4\pi^{*2}$, $^3\Sigma^-_{0^+}$ (2)
	3.50	$3\sigma^24\sigma^*\pi^4\pi^{*3}$, $^3\Pi_{0^+}$ (52.7); $3\sigma^24\sigma^{*2}\pi^4\pi^{*2}$, $^3\Sigma^-_{0^+}$ (28.8); $3\sigma^2\pi^4\pi^{*4}$, $^1\Sigma^+_{0^+}$ (12.5)
	4.00	$3\sigma^24\sigma^{*2}\pi^4\pi^{*2}$, $^3\Sigma^-_{0^+}$ (53.7); $3\sigma^24\sigma^*\pi^4\pi^{*3}$, $^3\Pi_{0^+}$ (35.5); $3\sigma^2\pi^4\pi^{*4}$, $^1\Sigma^+_{0^+}$ (4.7)
	8.00	$3\sigma^24\sigma^{*2}\pi^4\pi^{*2}$, $^3\Sigma^-_{0^+}$ (57); $3\sigma^24\sigma^*\pi^4\pi^{*3}$, $^3\Pi_{0^+}$ (36); $3\sigma^2\pi^4\pi^{*4}$, $^1\Sigma^+_{0^+}$ (4.2)
0^+(II)	2.50	$3\sigma^24\sigma^*\pi^4\pi^{*3}$, $^3\Pi_{0^+}$ (90); $3\sigma^2\pi^4\pi^{*4}$, $^1\Sigma^+_{0^+}$ (3)
	2.75	$3\sigma^24\sigma^*\pi^4\pi^{*3}$, $^3\Pi_{0^+}$ (94)
	3.00	$3\sigma^2\pi^4\pi^{*4}$, $^1\Sigma^+_{0^+}$ (52); $3\sigma^24\sigma^*\pi^4\pi^{*3}$, $^3\Pi_{0^+}$ (39)
	4.00	$3\sigma^24\sigma^*\pi^4\pi^{*3}$, $^3\Pi_{0^+}$ (45); $3\sigma^24\sigma^{*2}\pi^4\pi^{*2}$, $^3\Sigma^-_{0^+}$ (37.7); $3\sigma^2\pi^4\pi^{*4}$, $^1\Sigma^+_{0^+}$ (7.8)
	6.00	$3\sigma^24\sigma^*\pi^4\pi^{*3}$, $^3\Pi_{0^+}$ (94)
0^+(III)	2.50	$3\sigma^24\sigma^{*2}\pi^4\pi^{*2}$, $^3\Sigma^-_{0^+}$ (82.4); $3\sigma^2\pi^4\pi^{*4}$, $^1\Sigma^+_{0^+}$ (7.6)
	3.00	$3\sigma^24\sigma^*\pi^4\pi^{*3}$, $^3\Pi_{0^+}$ (46); $3\sigma^2\pi^4\pi^{*4}$, $^1\Sigma^+_{0^+}$ (39); $3\sigma^24\sigma^{*2}\pi^4\pi^{*2}$, $^3\Sigma^-_{0^+}$ (8.8)
	4.00	$3\sigma^2\pi^4\pi^{*4}$, $^1\Sigma^+_{0^+}$ (38.9); $3\sigma4\sigma^{*2}\pi^4\pi^{*3}$, $^3\Pi_{0^+}$(II) (38); $3\sigma^24\sigma^{*2}\pi^3\pi^{*3}$, $^1\Sigma^+_{0^+}$(III) (11)
2(I)	2.50	$3\sigma^24\sigma^*\pi^4\pi^{*3}$, $^3\Pi_2$ (94)
	3.00	$3\sigma^24\sigma^*\pi^4\pi^{*3}$, $^3\Pi_2$ (93)
	3.50	$3\sigma^24\sigma^*\pi^4\pi^{*3}$, $^3\Pi_2$ (92)
	4.00	$3\sigma^24\sigma^*\pi^4\pi^{*3}$, $^3\Pi_2$ (89); $3\sigma^24\sigma^{*2}\pi^4\pi^{*2}$, $^1\Delta_2$ (5)
	6.00	$3\sigma^24\sigma^*\pi^4\pi^{*3}$, $^3\Pi_2$ (91.4); $3\sigma^24\sigma^{*2}\pi^4\pi^{*2}$, $^1\Delta_2$ (6.6)
2(II)	2.50	$3\sigma^24\sigma^{*2}\pi^4\pi^{*2}$, $^1\Delta_2$ (90)
	3.00	$3\sigma^24\sigma^{*2}\pi^4\pi^{*2}$, $^1\Delta_2$ (87); $3\sigma^24\sigma^*\pi^4\pi^{*3}$, $^3\Pi_2$ (5)
	4.00	$3\sigma^24\sigma^{*2}\pi^4\pi^{*2}$, $^1\Delta_2$ (78.2); $3\sigma^24\sigma^*\pi^4\pi^{*3}$, $^3\Pi_2$ (18)
0^-	2.50	$3\sigma^24\sigma^*\pi^4\pi^{*3}$, $^3\Pi_{0^-}$ (94.1)
	3.00	$3\sigma^24\sigma^*\pi^4\pi^{*3}$, $^3\Pi_{0^-}$ (94.3)
	3.50	$3\sigma^24\sigma^*\pi^4\pi^{*3}$, $^3\Pi_{0^-}$ (95.5)
	4.00	$3\sigma^24\sigma^*\pi^4\pi^{*3}$, $^3\Pi_{0^-}$ (95)
	8.00	$3\sigma^24\sigma^*\pi^4\pi^{*3}$, $^3\Pi_{0^-}$ (98)
1(I)	2.50	$3\sigma^24\sigma^*\pi^4\pi^{*3}$, $^3\Pi_1$ (80.8); $3\sigma^24\sigma^*\pi^4\pi^{*3}$, $^1\Pi_1$ (12.3)
	3.00	$3\sigma^24\sigma^*\pi^4\pi^{*3}$, $^3\Pi_1$ (77.6); $3\sigma^24\sigma^*\pi^4\pi^{*3}$, $^1\Pi_1$ (12); $3\sigma^24\sigma^{*2}\pi^4\pi^{*2}$, $^3\Sigma^-_1$ (3)
	3.50	$3\sigma^24\sigma^*\pi^4\pi^{*3}$, $^3\Pi_1$ (69.7); $3\sigma^24\sigma^*\pi^4\pi^{*3}$, $^1\Pi_1$ (11.1); $3\sigma^24\sigma^{*2}\pi^4\pi^{*2}$, $^3\Sigma^-_1$ (13.8)
	4.00	$3\sigma^24\sigma^*\pi^4\pi^{*3}$, $^3\Pi_1$ (56.7); $3\sigma^24\sigma^*\pi^4\pi^{*3}$, $^1\Pi_1$ (9.5); $3\sigma^24\sigma^{*2}\pi^4\pi^{*2}$, $^3\Sigma^-_1$ (28.2)
	8.00	$3\sigma^24\sigma^*\pi^4\pi^{*3}$, $^3\Pi_1$ (52.3); $3\sigma^24\sigma^*\pi^4\pi^{*3}$, $^1\Pi_1$ (8.9) $3\sigma^24\sigma^{*2}\pi^4\pi^{*2}$, $^3\Sigma^-_1$ (36.8)
1(II)	3.50	$3\sigma^24\sigma^{*2}\pi^4\pi^{*2}$, $^3\Sigma^-_1$ (96)
	4.00	$3\sigma^24\sigma^{*2}\pi^4\pi^{*2}$, $^3\Sigma^-$ (96.8)
1(III)	4.00	$3\sigma^24\sigma^*\pi^4\pi^{*3}$, $^1\Pi_1$ (87.4); $3\sigma^24\sigma^*\pi^4\pi^{*3}$, $^3\Pi_1$ (7.2)
	8.00	$3\sigma^24\sigma^*\pi^4\pi^{*3}$, $^1\Pi_1$ (91); $3\sigma^24\sigma^*\pi^4\pi^{*3}$, $^3\Pi_1$ (6.9)

crossing of the corresponding 0^+ components as evidenced from Table VI. At 3.00 Å, 0^+(I) is a 53–38 % mixture of $^1\Sigma^+$ and $^3\Pi$. At 3.5 Å, the 0^+(I) state becomes predominantly $^3\Pi_{0^+}$ as expected since $^3\Pi$ is lower than $^1\Sigma^+$ at these distances (see Fig. 3). At longer distances there is one more avoided crossing since $^3\Pi_{0^+}$ dissociates into $Xe(^1S_0)+I^+(3P_0)$, while the $^3\Sigma^-_{0^+}$ curve dissociates into $Xe(^1S_0)+I^+(^3P_2)$.

The 0^+(III) state is predominately $^3\Sigma^-_{0^+}$ at 2.50 Å, although mixing with $^1\Sigma^+_{0^+}$ is non-negligible at this distance. As R increases to 3.00 Å, there is an avoided crossing between $^3\Pi_{0^+}$ and $^3\Sigma^-_{0^+}$. At 4.00 Å, the 0^+(III) state becomes a mixture of $^1\Sigma^+$ and $^3\Pi_{0^+}$. At longer distances the $^1\Sigma^+$ states dominates in the 0^+(III) state as it dissociates into $Xe(^1S)+I^+(^1D_2)$.

The 2(I) and 2(II) states stay relatively pure as a function of distance since there is no other 2 state in the vicinity of $^3\Pi_2$. At longer distances the mixing of $^3\Pi_2$ and $^1\Delta_2$ becomes more significant. The 0^- state is also pure $^3\Pi_{0^-}$ as there is no other state to mix with $^3\Pi_{0^-}$.

The 1(I) state is predominately $^3\Pi_1$ at most of the distances. However, $^3\Pi$-$^1\Pi$ mixing is very noticeable at all distances. The mixing of $^3\Sigma^-_1$ at $R>3.50$ Å becomes substantial as these two states are very close in this region. The 1(II) and 1(III) states are predominately $^3\Sigma^-_1$ and $^1\Pi_1$, respectively (see Table VI for exact compositions).

VI. CONCLUSIONS

In this investigation both experimental and theoretical studies were made on energy transfers in collisions of I^+ with Xe. Energy-transfer processes were modeled through the Landau-Zener model, which suggests efficient transfer of translational to electronic energies at the points of intersection of potential-energy curves of $(XeI)^+$. CASSCF followed by FOCI and RCI calculations were made on eight electronic states dissociating into $Xe(^1S_g)+I^+(^3P_g)$, $Xe(^1S_g)+I^+(^1D_g)$, and $Xe^+(^2P_u)+I(^2P_u)$ limits in the absence of spin-orbit interaction. Potential-energy curves of nine electronic states, which included spin-orbit effects, were also obtained. Theoretical potential-energy curves explain the observed $I^+(^1D_2)\leftrightarrows I^+(^3P_0,^3P_1)$ transfer and why the $I^+(^1D_2)\leftrightarrows I^+(^3P_2)$ transition could not be observed. Theoretical calculations indicate that XeI^+ is bound and long lived. The D_e of two bound 0^+ states are estimated as 1.0±0.2 and 0.7±0.2 eV, respectively. Mulliken population analyses of low-lying states reveals that the positive charge is predominantly on I in $^3\Sigma^-$ and $^3\Pi$ states, while it is equitably split between Xe and I in the $^1\Sigma^+$ and $^1\Pi$ states. The analyses of RCI wave functions reveal a number of avoided crossings in the 0^+ curves, which result in the distribution of the binding energy of $^1\Sigma^+$ state into two 0^+ states.

ACKNOWLEDGMENTS

One of us (K.B.) thanks the National Science Foundation for a partial support of this research through Grant No. CHE88-18869 and through the Camille and Henry Dreyfus Foundation. We are indebted to Professor John B. Delos for critically reading this manuscript and for an illuminating discussion of the Landau-Zener process. The authors also thank the San Diego Super Computing Center for providing part of the computing time required for this project.

[1]M. Hottoka, Bjorn Roos, J. B. Delos, R. Srivastava, R. B. Sharma, and W. S. Koski, Phys. Rev. A **35**, 4515 (1987).
[2]K. Balasubramanian, Pingyi Feng, Joyce J. Kaufman, P. C. Hariharan, and W. S. Koski, Phys. Rev. A **37**, 3204 (1988).
[3]Douglas A. Chapman, K. Balasubramanian, S. H. Lin, Joyce J. Daufman, P. C. Hariharan, and W. S. Koski, Phys. Rev. A **39**, 4428 (1989).
[4]K. Balasubramanian, Joyce J. Kaufman, P. C. Hariharan, and W. S. Koski, Chem. Phys. Lett. **114**, 201 (1985).
[5]H. P. Watkins and W. S. Koski, Chem. Phys. Lett. **77**, 470 (1981).
[6]K. Wendell, C. A. Jones, J. J. Kaufman, and W. S. Koski, J. Chem. Phys. **63**, 750 (1975).
[7]L. G. Piper, J. E. Velazco, and D. W. Setser, J. Chem. Phys. **59**, 3323 (1973).
[8]J. E. Velazco, J. H. Kohs, and D. W. Setser, J. Chem. Phys. **65**, 3468 (1976).
[9]D. L. King, L. G. Piper, and D. W. Setser, J. Chem. Soc. Faraday Trans. 3 **73**, 177 (1977).
[10]M. Rokini, J. H. Jacobs, and J. A. Mangano, Phys. Rev. A **16**, 2216 (1977).
[11]R. E. Olson and B. Liu, Phys. Rev. A **17**, 1568 (1978).
[12]T. H. Dunning and P. J. Hay, J. Chem. Phys. **66**, 3767 (1977).
[13]J. S. Cohen, W. R. Wadt, and P. J. Hay, J. Chem. Phys. **71**, 2955 (1979).
[14]J. H. Holloway, *Noble Gas Chemistry* (Methuen, London, 1968).
[15]A. Henglein and G. A. Muccini, Angew. Chem. **72**, 630 (1960).
[16]I. Kuen and F. Howorka, J. Chem. Phys. **70**, 595 (1979).
[17]J. Berkowitz and J. H. Holloway, J. Chem. Soc. Faraday Trans. 3 **74**, 2707 (1978).
[18]J. Berkowitz, W. A. Chupka, R. L. Guyon, J. H. Holloway, and R. Sphor, J. Phys. Chem. **75**, 1461 (1971).
[19]L. A. La John, P. A. Christiansen, R. B. Ross, T. Atashroo, and W. C. Ermler, J. Chem. Phys. **87**, 2812 (1987).
[20]K. Balasubramanian, Chem. Phys. Lett. **127**, 585 (1986).
[21]The major authors of ALCHEMY II are B. Liu, B. Lengsfield and M. Yoshimine.
[22]R. M. Pitzer and N. W. Winter, J. Phys. Chem. **92**, 3061 (1988).
[23]K. Balasubramanian, J. Chem. Phys. **89**, 5731 (1988).
[24]C. E. Moore, *Table of Atomic Energy Levels*, Natl. Bur. Stand. (U.S.) Circ. No. 467 (U.S. GPO, Washington, D.C., 1971), Vol. 3.
[25]J. Q. Li and K. Balasubramanian, J. Mol. Spectrosc. **138**, 162 (1989).